UNACYLATED GHRELIN REDUCES SKELETAL MUSCLE REACTIVE OXYGEN SPECIES GENERATION AND INFLAMMATION AND PREVENTS HIGH-FAT DIET INDUCED HYPERGLYCEMIA AND WHOLE-BODY INSULIN RESISTANCE IN RODENTS

Gianluca Gortan Cappellari[1], Michela Zanetti[1], Annamaria Semolic[1], Pierandrea Vinci[1], Giulia Ruozi[2], Antonella Falcione[2], Nicoletta Filigheddu[3], Gianfranco Guarnieri[1], Andrea Graziani[3,4], Mauro Giacca[2], Rocco Barazzoni[1]

[1]Department of Medical, Surgical and Health Sciences – University of Trieste, Trieste, Italy

[2]Molecular Medicine Lab., International Centre for Genetic Engineering and Biotechnology, Trieste, Italy

[3]Department of Translational Medicine, Università del Piemonte Orientale "Amedeo Avogadro, Novara, Italy

[4]Medical School, Università Vita e Salute San Raffaele, Milan, Italy

Corresponding author: Rocco Barazzoni

UCO Clinica Medica – Ospedale di Cattinara
Strada di Fiume 447
34149 Trieste – Italy
Phone: 39-0403994416
e-mail: barazzon@units.it

Running title: Unacylated ghrelin and muscle metabolism

Word count: 3969, Tables: 0, Figures: 8, Supplementary Figures: 3

Diabetes Publish Ahead of Print, published online January 28, 2016

Abstract

Excess reactive oxygen species (ROS) generation and inflammation may contribute to obesity-associated skeletal muscle insulin resistance. Ghrelin is a gastric hormone whose unacylated (UnAG) form is associated with whole-body insulin sensitivity in humans and may reduce oxidative stress in non-muscle cells in-vitro. We hypothesized that UnAG 1) lowers muscle ROS production and inflammation and enhances tissue insulin action in lean rats; 2) prevents muscle metabolic alterations and normalizes insulin resistance and hyperglycemia in high-fat diet (HFD)-induced obesity. In 12-week-old lean rats, UnAG (4-day, twice-daily subcutaneous 200µg-injections) reduced gastrocnemius mitochondrial ROS generation and inflammatory cytokines while enhancing AKT-dependent signaling and insulin-stimulated glucose uptake. In HFD-treated mice, chronic UnAG overexpression prevented obesity-associated hyperglycemia and whole-body insulin resistance (insulin-tolerance test), as well as muscle oxidative stress, inflammation and altered insulin signalling. In myotubes, UnAG consistently lowered mitochondrial ROS production and enhanced insulin signalling, while UnAG effects were prevented by siRNA-mediated silencing of the autophagy mediator ATG5. Thus, UnAG lowers mitochondrial ROS production and inflammation while enhancing insulin action in rodent skeletal muscle. In HFD-induced obesity, these effects prevent hyperglycemia and insulin resistance. Stimulated muscle autophagy could contribute to UnAG activities. These findings support UnAG as a therapeutic strategy for obesity-associated metabolic alterations.

Introduction

Clustered metabolic abnormalities including excess reactive oxygen species (ROS) generation and inflammation activation are proposed contributors to the onset of skeletal muscle insulin resistance (1-5). Excess muscle ROS production and inflammation are indeed linked at the level of IκB/NF-κB activation and may cause insulin resistance by inhibiting insulin signalling downstream of insulin receptor (2,3,5). Ghrelin is a peptide hormone predominantly secreted by the stomach whose acylated form (AG) is a major hypothalamic orexigenic signal (6,7). Sustained AG administration causes weight gain and hyperglycemia despite enhanced muscle mitochondrial oxidative capacity (8,9) by increasing food intake, hepatic gluconeogenesis and fat deposition in rodents (10,11). A comprehensive understanding of the metabolic impact of ghrelin has been however recently allowed by reports of independent more favourable effects of its unacylated form (UnAG). Although no specific UnAG receptor has been yet identified, UnAG counteracts glucogenic effects of AG as well as AG-induced hyperglycemia (10), and negative associations have been reported between circulating UnAG and markers of whole-body insulin resistance in humans (12,13). Emerging antioxidant effects have been interestingly reported for UnAG in different cell types (14-17) and we recently demonstrated that UnAG stimulates autophagy in rodent muscle, thereby also potentially lowering muscle oxidative stress through disposal of damaged mitochondria (18). No information is however available 1) on the impact of UnAG on skeletal muscle ROS generation, inflammation and insulin action; 2) on whether UnAG prevents altered oxidative stress, inflammation and insulin action in obesity and diabetes.

We therefore studied lean rats and a transgenic mouse model of systemic UnAG overproduction (19) to test the hypothesis that UnAG 1) lowers mitochondrial ROS production and inflammation and enhances insulin action in lean rodent muscle; 2) normalizes high-fat diet (HFD)-induced

muscle metabolic alterations, whole-body insulin resistance and hyperglycemia. In addition, effects of UnAG were verified in vitro in myotubes, where we also mechanistically tested the hypothesis that UnAG activites are at least partly mediated by positive modulation of autophagy.

Research Design and Methods

Experimental design

Exogenous UnAG administration Experiments were approved by the Animal Studies Committee at Trieste University. Twenty 12-week-old male Wistar rats (Harlan-Italy, San Pietro-al-Natisone, Udine, Italy) were housed for two weeks in individual cages with a 12-h light–dark cycle at the University Animal Facility, with ad-libitum water and standard chow (Harlan 2018, 14.2 kJ/g). Animals were then randomly assigned to 4-day, twice-daily 200µg-subcutaneous injections of UnAG (n=10, Bachem, Bubendorf, CH) or vehicle (Ct, n=10, NaCl 0,9% w/v). UnAG dose was based on previous studies in which equimolar AG modulated the same parameters (8). Body weight and food intake were monitored daily; after the last injection, food was removed for three hours followed by anaesthesia (Tiobutabarbital 100 mg/kg, Tiletamine/Zolazepam (1:1) 40 mg/kg IP). Gastrocnemius and extensor digitorum longus (EDL) muscles were then surgically isolated and blood collected by heart puncture.

Transgenic UnAG overexpression Generation and characteristics of transgenic mice overexpressing UnAG (Tg Myh6/Ghrl) were previously described (19). Selective ghrelin overproduction in the heart, characterized by negligible acylating activity, results in 40-fold increment in circulating UnAG without AG modification. 14 Tg Myh6/Ghrl and 14 matched wild-type male mice underwent 16-week standard or HFD feeding (10% or 60% calories from fat; Research Diets, New Brunswick, NJ), and were sacrificed as described above. Insulin tolerance tests (ITT) were performed at 15 weeks of treatment by intraperitoneal insulin injection (Humulin-R, Lilly, Indianapolis, IN; 3 nmol/kg) after 4-h fasting. Blood glucose was measured from tail blood (AccuCheck Active, Roche, Basel, CH) immediately prior to injection and at 20, 40, 60, 80 min.

Myotube experiments C2C12 myoblasts were differentiated in myotubes (20). After 4-day incubation with differentiation medium and 18h-starvation, cells were treated with AG or UnAG (0.1, 0.5, 1µmol/l) for 48 h, collected and processed. In additional experiments, the potential role of autophagy in effects of UnAG was investigated by genomic silencing of the autophagy mediator ATG5 (18). SiRNA knockdown of ATG5 was performed by reverse transfection at final 25nM concentration with mouse ATG5 siRNA (M-064838-02-0005; Dharmacon) or with a non-targeting control siRNA #4 (D-001210-04-20; Dharmacon) using Lipofectamine RNAiMAX (Life Technologies). Twenty-four hours after transfection, culture medium was replaced and after thirty-six hours differentiated, treated and processed as above. ATG5 protein levels were quantified by western blot.

Analytical methods

Plasma insulin and non-esterified fatty acids (NEFA) Plasma insulin concentration was measured by ELISA (Ultrasensitive ELISA, DRG, Springfield, NJ). Plasma glucose and NEFA were determined by standard enzymatic-colorimetric assays (21,22).

Ex vivo redox state Mitochondrial H_2O_2 production was assessed in isolated intact mitochondria from tissues and cells using the Amplex Red (10µmol/l, Invitrogen, Carlsbad, CA)-HRP method, modified as previously reported and normalised by citrate synthase (CS) activity in the same mitochondrial preparation (22,23). Assay substrate concentrations (mmol/l) were: 8 glutamate, 4 malate (GM); 10 succinate (S); 4 glutamate, 2 malate, 10 succinate (GMS); 0.05 palmitoyl-L-carnitine, 2 malate (PCM). Superoxide anion production sources in gastrocnemius muscle whole-tissue homogenate were assessed using the lucigenin chemiluminescent method as described (22) and normalised by protein concentration (BCA assay, Pierce, Rockford IL, USA). The impact of subsequent addition of specific inhibitors on specific substrate-stimulated production rates was

used to evaluate relative superoxide production from each source (Mitochondria: 5µmol/l CCCP on Succinate; NOS: 10mmol/l L-NAME on 10mmol/l L-Arginine; NADPH Oxidase: 200µmol/l DPI on 1mmol/l NADPH; Xanthine oxidase: 200µmol/l Oxypurinol on 500µmol/l Xanthine) as referenced.

Glutathione and antioxidant enzyme activities Total and oxidised glutathione were determined as referenced (24) on ~50mg of gastrocnemius cleaned and homogenised in ice-cold 5% (wt/vol.) metaphosphoric acid (20ml/g tissue). Reduced glutathione (GSH) was calculated as total minus oxidised fraction (GSSG). Commercial kits were used to measure catalase (Amplex Red Catalase Assay, Invitrogen, Carlsbad, CA) and glutathione peroxidase activities (Abcam, Cambridge, UK).

Protein analyses

-xMAP Cytokine profile and insulin signalling protein phosphorylation at $IR^{Y1162/Y1163}$, IRS-1^{S312}, AKT^{S473}, GSK-$3\beta^{S9}$, $PRAS40^{T246}$ and $P70S6K^{T421/S424}$ levels were measured by xMAP technology (Magpix, Luminex Corporation, Austin, TX) using commercial kits, validated by manufacturer for multiplexing profiling (LRC0002M; LHO0001M; LHO0002, Life Technologies, Carlsbad, CA). Milliplex Analyst software (Millipore, Billerica, MA) was used for interpolating data to standard curve. Phosphorylation of each protein is expressed as phospho-protein units/total pg.

-Western Blot Western Blots were performed as described (21,22,25). Equal loading was checked by Ponceau-S staining and GAPDH reprobing. Primary antibodies dilutions were: anti-MnSuperoxide Dismutase (SOD) and anti-CuZnSOD (Stressgen, Ann Arbor, MI) 1:5000 and 1:1000 respectively; anti-IκB (Cell Signaling, Beverly, MA) 1:500; anti-pIRS-1^{Y612} (Abcam,

Cambridge, UK) 1:500; anti-ATG5 (Cell Signaling) 1:2000; anti LC3B (Sigma) 1:1500; anti-b-Actin (Sigma) 1:25000 and anti-GAPDH (Santa Cruz, Dallas, TX) 1:1000.

Electrophoretic mobility shift assay (EMSA) NF-κB binding activity was assessed by non-radioactive EMSA (22) with modifications. Equal amounts of nuclear protein were loaded for each sample. After incubation with polydeoxyinosinic-deoxycytidylic acid (0.05μg/μl) and double-stranded 3′-biotinylated DNA probe, electrophoretic separation of nuclear extracts was performed in 0.8% agarose gel. Band specificity evaluation and identification was performed by running a pooled sample pre-incubated for 20 min with excess unlabelled probe (1000x), anti-p65 (Millipore; 2μg) or anti-p105/p50 (Abcam; 2μg) antibody. Results were calculated from optical density of NF-κB specific bands.

Tissue Glucose uptake Tissue glucose uptake was measured ex-vivo with non-radioactive 2-deoxyglucose (2-DG) (26). EDL muscle is metabolically largely similar to gastrocnemius (27) and was used because of smaller diameter and better exchange with incubation buffer (28). Two muscle sections were incubated for 30’ at 37°C under constant oxygenation with or without insulin (Humulin-R 600pmol/l) in isotonic buffer, pH=7.4, added with BSA (1mg/ml) and pyruvate (2mM). After 20-min incubation with pyruvate substituted with 2-DG (1mM), samples were snap frozen and kept at -80°C. After homogenization in ultrapure water followed by NaOH addition (0.07N), enzymes and endogenous NAD(P)H and NAD(P) were inactivated by 45-min incubation at 85°C. Equinormal quantities of HCl were then added, samples were cleared from debris by centrifugation (10000xg, 5min) and transferred to 96-well microplates for incubation (37°C, 60min) in assay buffer, added with (Buffer C) β-NADP (0.1mM) and Glucose-6-phosphate dehydrogenase from L. Mesenteroides (G6PDH, 20U/ml) or (Buffer D) with β-NAD 0.1mM and G6PDH (0.3U/ml). Concentrations of G6P and G6P+2-DG6P were quantified by

fluorimetrically measuring (Infinite F200, Tecan, Männedorf, CH) conversion of Resazurin in Resorufin in Buffers C and D, respectively. Values related to 2-DG6P were calculated by subtraction, interpolated on a standard curve of 2-DG6P, and normalized by protein concentration in sample homogenate. Tissue 2-DG6P uptake was expressed in µmol of 2-DG/mg protein/30min.

ATP synthesis and complex-related ATP production ATP synthesis rate was measured in tissues and cells ex-vivo in freshly isolated mitochondria using a luciferin-luciferase luminometric assay (22). Integrity of mitochondria isolated by gentle homogenization was tested by comparison of citrate synthase measurements in samples before and after membrane disruption (29). After signal stabilization and excess substrates addition a first 10-min kinetic read was performed, followed by 100µmol/l ADP addition and 20-min read. Final respiration substrates composition and reaction concentrations (mmol/l) were: 0.25 pyruvate, 0.0125 palmitoyl-L-carnitine, 2.5 α-ketoglutarate, 0.25 malate (PPKM); 0.025 palmitoyl-L-carnitine, 0.5 malate (PCM); 20 succinate, 0.1 rotenone (SR); 10 glutamate, 5 malate (GM). The impact of complex-related energy flux on ATP synthesis was calculated as the difference in production rate induced by the addition, in a subsequent 20-min read, of a complex-specific inhibitor during state-3 respiration on excess complex-specific substrate. For complex I-related ATP synthesis, substrate and inhibitor were GM and rotenone (2µmol/l), while for complex II SR and malonate (1mmol/l). Mitochondrial functional integrity in each preparation was confirmed by a >80% and >95% decrease in state 3 ATP synthesis after addition of CCCP 30µM and oligomycin 2µg/µl respectively. Values were then normalized by ATP synthesis rate with the non-specific substrate PPKM, and data presented as the ratio between values obtained for complex I-related over complex II-related results.

Statistical analysis Groups were compared using Student t-test or one-way ANOVA followed by appropriate post-hoc tests. Bonferroni correction for multiple comparisons was applied. $p<0.05$ was considered statistically significant.

Results

EXOGENOUS UnAG ADMINISTRATION

Animal characteristics In lean adult rats, exogenous 4-day UnAG did not modify body weight (Ct:319.6±3.6g; UnAG:324.1±6.1g), weight gain during treatment (Ct:13.0±1.4g; UnAG:11.6±1.1g) or caloric intake (Ct: 76.9±2.3kcal/d; UnAG: 73.5±1.8kcal/d). Plasma glucose (Ct: 118.6±6.0mg/dL; UnAG: 120.5±7.5mg/dL), insulin (Ct: 12.8±2.1μU/ml; UnAG: 14.3±2.9μU/ml) and NEFA (Ct: 0.27±0.06mmol/L; UnAG: 0.21±0.03mmol/L) concentrations were comparable among groups.

UnAG lowers skeletal muscle ROS production UnAG lowered gastrocnemius H_2O_2 and superoxide anion production rate, and this effect involved mitochondrial respiration-dependent ROS generation (Figure1A-C). NOS-dependent but not xanthine- or NADPH oxidase-dependent superoxide production was also reduced by UnAG (Figure 1D-F). UnAG-treated rats also had lower muscle oxidized-over-total glutathione, a marker of tissue redox state (Figure 1G-H). Tissue protein levels of SOD isoforms and activities of antioxidant catalase and glutathione peroxidase were conversely not modified by UnAG (Figure 1I-L).

UnAG lowers tissue inflammation Protein expression of the NF-κB inhibitor IκB was higher in UnAG- compared to saline-treated rats, with parallel reduction of pro-inflammatory NF-κB p65/p50 nuclear binding activity (Figure 2A-B). UnAG also increased p50/p50 homodimer binding activity (Figure 2B), a transcription activator for anti-inflammatory IL-10 (30). UnAG

treatment consistently resulted in anti-inflammatory changes in muscle cytokine patterns, with higher IL-10 expression and lower pro-inflammatory IL-1a and TNFα (Figure 2C-G).

UnAG enhances insulin signalling and glucose uptake UnAG also led to insulin signaling activation with increased phosphorylation of AKT^{S473}, $GSK\text{-}3\beta^{S9}$, $PRAS40^{T246}$ and $P70S6K^{T421/S424}$ (Figure 3A-F), consistent with activation of both mTORC complexes kinase activity. Changes in insulin signalling were paralleled by higher insulin-stimulated muscle glucose uptake (Figure 3G). These effects were further associated with enhanced $IRS\text{-}1^{S312}$ phosphorylation (Figure 3B), an mTORC-dependent negative feedback mechanism and marker for enhanced insulin signaling (31). To determine whether activating IRS-1 phosphorylations were also enhanced, we measured $pIRS\text{-}1^{Y612}$ and found no stimulation in UnAG-treated animals (Supplementary Figure 1A), further indicating that UnAG-associated activation of insulin signalling occurs downstream of mTORC complexes but not at IR-IRS1 level.

In vivo effects of UnAG are tissue-specific In liver tissue, a non-statistically significant reduction in mitochondrial superoxide production was observed. This relatively minor change was not associated with altered redox state, inflammation markers or insulin signalling (Supplementary Figures 2A-I, 3A-F), as previously shown (32,33).

TRANSGENIC UnAG OVEREXPRESSION AND HFD-INDUCED OBESITY

Animal characteristics Up-regulation of circulating UnAG by myocardial overexpression of the ghrelin gene (Tg Myh6/Ghrl) (19) did not modify body weight (Control-Diet: Ct: 31.0±2.1g; Tg Myh6/Ghrl: 28.7±2.1g; HFD: Ct: 37.9±3.0g; Tg Myh6/Ghrl: 36.6±1.1g) or caloric intake (Control-Diet: Ct: 13.5±0.1kcal/d; Tg Myh6/Ghrl: 14.6±0.6kcal/d; HFD: Ct: 17.6±0.1kcal/d; Tg Myh6/Ghrl: 17.9±0.5kcal/d) under any dietary regimen (19). Blood glucose (Control Diet: Ct:

106.0±7.3mg/dL; Tg Myh6/Ghrl: 98.2±8.0mg/dL), plasma insulin (Control Diet: Ct: 13.3±1.8μU/ml; Tg Myh6/Ghrl: 14.5±3.1μU/ml;) and NEFA (Control Diet: Ct: 0.32±0.06mmol/L; Tg Myh6/Ghrl: 0.38±0.08mmol/L) were also comparable among lean groups. In contrast, blood glucose (HFD Ct: 161.9±30.7mg/dL; Tg Myh6/Ghrl: 102.7±11.6mg/dL; P<0.05 Ct vs Tg Myh6/Ghrl) and plasma insulin (HFD: Ct: 25.1±2.2μU/ml; Tg Myh6/Ghrl: 16.5±1.6μU/ml; P<0.05 Ct vs Tg Myh6/Ghrl) while not NEFA (HFD: Ct: 0.27±0.05mmol/L; Tg Myh6/Ghrl: 0.32±0.10mmol/L; P=NS) were lower in HFD-obese Tg Myh6/Ghrl compared to both wild-type HFD animals and lean groups (P=NS HFD Tg Myh6/Ghrl vs lean groups).

Systemic circulating UnAG up-regulation prevents obesity-associated hyperglycemia, whole-body insulin resistance and skeletal muscle oxidative stress, inflammation and impaired AKT phosphorylation Consistent with exogenous UnAG administration, circulating UnAG up-regulation in Tg Myh6/Ghrl was characterized by lower muscle oxidized-to-total glutathione, less pro-inflammatory tissue cytokine profile and more pronounced phosphorylation of AKT^{S473}, GSK-$3\beta^{S9}$, $PRAS40^{T246}$ and $P70S6K^{T421/S424}$ (Figure 4A-M). These effects were associated with higher insulin sensitivity by area-under-the-curve (AUC) for ITT-induced blood glucose changes (Figure 4N-P). Obese wild-type animals were expectedly hyperglycemic and insulin resistant (Figure 4N-P). The obese wild-type group also had higher oxidized-to-total glutathione, pro-inflammatory cytokine profile and reduced phosphorylation of AKT^{S473} and GSK-$3\beta^{S9}$ in gastrocnemius (Figure 4A-M). Compared to lean Tg Myh6/Ghrl, obese Tg Myh6/Ghrl had moderately higher muscle oxidized-to-total glutathione and TNFα, that however remained lower (P<0.05) than obese and comparable (P=NS) to lean wild-type animals (Figure 4B,4E). In addition, UnAG upregulation prevented obesity-associated increments (P<0.05 vs obese wild-type) in muscle pro-inflammatory cytokines IL-1α and IL-1β with lower IL-6, and resulted in

normalized activating phosphorylation at AKT^{S473} and GSK-3β^{S9} levels (P=NS vs lean Tg Myh6/Ghrl). Importantly, obese Tg Myh6/Ghrl were protected from obesity-induced hyperglycemia and whole-body insulin resistance (Figure 4N-P), with both parameters superimposable to lean wild-type animals. Insulin signalling proteins upstream of AKT were not activated in Tg Myh6/Ghrl, with patterns of pIRS-1^{S312} and pIRS-1^{Y612} comparable to those observed in exogenously-treated animals (Figure 4H-I, Supplementary Figure 1B).

IN VITRO MYOTUBE EXPERIMENTS

UnAG effects on ROS production and insulin signalling are confirmed in C2C12 myotubes 48-hour UnAG treatment of C2C12 myotubes lowered mitochondrial ROS generation with largely dose-dependent effects (Figure 5A). Also consistently with in vivo data, UnAG resulted in increased activating phosphorylation of mTORC complexes-dependent insulin signaling proteins AKT^{S473}, GSK-3β^{S9}, PRAS40^{T246} and P70S6K$^{T421/S424}$. Patterns of pIR$^{Y1162/Y1163}$ and pIRS-1^{S312} were also comparable in C2C12 and in-vivo experiments, supporting lack of activation of IR-IRS1 (Figure 5B-G).

UnAG effects in vitro are not shared by AG C2C12 myotubes do not appear to express the AG receptor GHSR1 (34). To further exclude the possibility that UnAG-induced changes result from non-specific activation of additional AG-regulated pathways, C2C12 experiments were performed with equimolar AG concentrations. 48-hour AG incubation failed to inhibit ROS production and to activate insulin signalling except for less pronounced enhancement of pGSK-3β^{S9} (Figure 5A-G).

UnAG effects in vitro are abolished by silencing the autophagy mediator ATG5 In additional experiments, C2C12 myotubes were incubated with UnAG after genomic silencing of the autophagy mediator ATG5. ATG5 silencing abolished UnAG activities on both mitochondrial ROS production and insulin signalling (Figure 6A-H). Levels of the autophagy activation marker LC3II/LC3I were also higher in HFD-obese Tg Myh6/Ghrl than wild-type mice (Figure 6I).

MITOCHONDRIAL ATP PRODUCTION

Effects of UnAG are not associated with enhanced skeletal muscle mitochondrial function Consistent with previous results (22,35), UnAG-induced changes in redox state, inflammation and insulin signalling were not associated with enhanced, but rather with lower or unchanged ATP production rate in vivo and in vitro respectively (Figure 7A-C). Higher skeletal muscle ATP production was observed in obese mice compared to lean counterparts, but UnAG up-regulation was associated with lower ATP production rates also in obese animals (Figure 7B). UnAG modified muscle respiratory chain complex-related ATP production by shifting ATP synthesis towards complex I over complex II both in vivo and in vitro (Figure 7D-E). Differently from UnAG, AG enhanced ATP production in C2C12 myotubes (Figure 7C). Liver ATP production was not modified by UnAG (Supplementary Figure 3G).

Discussion

These studies demonstrated that 1) sustained UnAG administration in vivo leads to a) lower muscle ROS production and less oxidized tissue redox state; b) anti-inflammatory changes in tissue NF-κB activation and cytokine patterns; c) enhanced mTORC-dependent insulin signalling with higher insulin-stimulated muscle glucose uptake. 2) Muscle effects of UnAG are

reproduced in a model of systemic circulating UnAG up-regulation with HFD-induced obesity, resulting in prevention of obesity-associated hyperglycemia and whole-body insulin resistance. 3) UnAG effects are dose-dependently confirmed in myotubes; differential effects of AG and UnAG are observed in vitro, thereby indicating that UnAG acts at least partly directly and independently of AG-regulated pathways. Finally, UnAG effects in vitro are abolished by autophagy inhibition, thereby indicating mechanistic involvement of autophagy in UnAG activities.

The current results show that UnAG negatively regulates skeletal muscle ROS production and inflammation, and these effects are indirectly supported by previous in vitro observations in non-muscle cells (14,16,19). In a recent study, UnAG reduced endothelial oxidative stress in models of peripheral artery disease by restoring SOD expression (15,16). Skeletal muscle SOD expression and antioxidant enzyme activities were however unchanged by UnAG in the current model, indicating lower mitochondrial ROS generation rather than enhanced antioxidant defenses as a key mediator of UnAG-induced muscle antioxidant activity. Since we recently identified UnAG as a potent inducer of autophagy in cardiomyocytes and myotubes (35), enhanced removal of dysfunctional mitochondria could have contributed to lower tissue oxidative load in the current experimental setting. This hypothesis was notably confirmed in myotubes experiments using siRNA-mediated autophagy inhibition. Among less quantitatively relevant ROS sources (36), UnAG selectively inhibited NOS-dependent superoxide production. This finding is intriguingly consistent with emerging co-localization and functional interactions between NOS, nitric oxide (NO) and muscle mitochondria (37,38). In particular, NO production has been reported to enhance mitochondrial ROS generation (37) while UnAG was reported to

reduce NO production induced by pro-inflammatory cytokines in various settings (39). Potential interactions between UnAG, NO and mitochondrial ROS generation should be directly investigated in future studies.

Sustained UnAG administration enhanced skeletal muscle insulin signalling downstream of mTORC complexes while not at IR-IRS-1 level, and these effects were paralleled by increased insulin-stimulated muscle glucose uptake. These changes are importantly in excellent agreement with, and provide a molecular basis for, clinical observations linking UnAG with preserved whole-body insulin sensitivity in humans (12,13). Interestingly, autophagy inhibition in vitro abolished UnAG activities on both mitochondrial ROS production and insulin signalling. These observations provide further strong support for a causal negative impact of mitochondrial ROS production on AKT-dependent insulin signalling, in agreement with previous observations (1-5). Intriguingly, UnAG effects were associated with enhanced inhibitory IRS-1^{S312} phosphorylation. This seemingly paradoxical observation is however consistent with recent reports of IRS-1^{S312} phosphorylation as a physiological negative feedback modulation following downstream signalling activation (31).

Results in Tg Myh6/Ghrl mice with chronic systemic UnAG over-exposure (19) confirmed effects of exogenous UnAG administration, and these results are supported by higher insulin sensitivity in a lean UnAG adipose transgenic model (17). Since plasma AG and IGF-1 are unchanged in Tg Myh6/Ghrl (19), our findings further confirm that UnAG effects are independent of changes in AG and its potential impact on GH-IGF1 through GHSR1 (7,19). Most importantly, circulating UnAG upregulation prevented HFD-induced hyperglycemia and systemic insulin resistance, while muscle oxidative stress markers, inflammation and impaired insulin signalling were overall preserved at levels comparable with lean Tg Myh6/Ghrl or wild-

type animals. UnAG-dependent stimulation of muscle autophagy was also confirmed in vivo in HFD-obese Tg Myh6/Ghrl by higher LC3II/LC3I ratio, and could therefore have potentially directly contributed to beneficial effects of UnAG overexpression (40). Interestingly, obese Tg Myh6/Ghrl animals showed no increments in pIRS-1^{S312} compared to wild-type counterparts, and lack of effect was associated with lack of stimulation of insulin signalling activation at P70S6K levels. These combined observations are consistent with the hypothesis that IRS-1^{S312} phosphorylation is at least partly mediated by this feedback loop (31). Potential mechanisms underlying differential regulation of PRAS40^{T246} and P70S6K$^{T421/S424}$ phosphorylation in obese vs lean models of UnAG exposure should be investigated in future studies. Overall, results in the HFD-obesity model importantly demonstrate that effects of UnAG translate into beneficial metabolic changes in a clinically relevant model of dietary-induced insulin resistance and hyperglycemia, thereby providing a strong rationale for therapeutic strategies to increase UnAG availability in obese, insulin resistant and type 2 diabetic conditions.

Myotubes experiments were in excellent agreement with in vivo studies in showing superimposable effects of UnAG on ROS production and insulin signalling, that were not induced by equimolar AG concentrations. These observations strongly indicate that UnAG directly stimulates skeletal muscle insulin signaling and they are consistent with previously-reported UnAG signaling and anti-atrophic activities in skeletal muscle of both wt and GHSR1 knockout mice (19). These findings overall provide strong support to the hypothesis that UnAG effects in skeletal muscle are independent of GHSR1 and are mediated by alternative, yet-unidentified UnAG receptor(s). It should also be pointed out that both AG and UnAG stimulate differentiation of C2C12 myoblasts (34), and that both ghrelin forms enhance mTORC2-mediated anti-atrophic signalling under acute experimental conditions in C2C12 myotubes as

well as in vivo in skeletal muscle of GHSR KO mice (19, 32). In the current studies with prolonged hormone incubation, highest AG doses selectively induced a moderate increase of GSK-3β^{S9} phosphorylation but they failed to reduce ROS generation and to enhance downstream insulin signaling. Also consistent with these findings, AG is a weaker autophagy inducer than UnAG and it fails to stimulate both mitophagy (35) and ischemia-induced skeletal muscle regeneration (15). Based on available knowledge, differential muscle effects of ghrelin forms may depend on still uninvestigated acylation-selective and time-dependent AG activities. Overall, differential effects of ghrelin forms on muscle insulin signalling are fully consistent with clinical observations linking UnAG, but not AG to whole-body insulin sensitivity in humans (12,13).

It should be finally pointed out that UnAG-induced lower ROS production, lower inflammation and enhanced insulin signalling were associated with reduced or unchanged ATP production. In agreement with previous studies, high-fat fed animals conversely showed higher mitochondrial ATP production despite higher oxidative stress markers and insulin resistance (32), and this alteration could involve enhanced substrate availability through feed-forward mechanisms (32). Our results therefore provide further evidence against a role for low mitochondrial function to primarily cause insulin resistance (41-45), conversely indicating UnAG as a novel modulator of muscle mitochondrial activity with negative impact on both ATP and ROS production in vivo. Unchanged mitochondrial ATP production in vitro however does not support a direct role of UnAG to inhibit mitochondrial function, while it further indicates that reduced mitochondrial function is not a prerequisite for reduced ROS generation. Interestingly, UnAG modified complex-related ATP production by favoring complex I over complex II-related synthesis in vitro and in vivo, potentially reflecting preferential glucose over fat-derived substrate oxidation

(46). Since glucose-related substrate oxidation may lower mitochondrial ROS generation (47,48), this mechanism could also contribute to inhibit ROS production. Further studies on interactions between UnAG and muscle mitochondrial function are warranted by the current results.

In conclusion, these studies demonstrated a novel role of UnAG to modulate skeletal muscle redox state, inflammation and insulin signalling. UnAG-treated rat muscle is characterized by lower mitochondrial ROS production, lower inflammation and enhanced insulin signalling and action. These effects are tissue-specific, they appear to be direct and independent of acylated hormone, and they could be at least partly mediated by UnAG-dependent stimulation of autophagy (Figure 8). UnAG overexpression also prevents obesity-associated hyperglycemia and systemic insulin resistance as well as muscle oxidative stress, inflammation activation and impaired insulin signalling. The current findings collectively indicate UnAG as a potential novel treatment for obesity-associated metabolic alterations.

Author Contributions

GGC performed experiments, researched and analyzed data and contributed to study design and writing of the manuscript, MZ contributed to discussion and reviewed/edited the manuscript, AS performed experiments and contributed to data analysis and discussion, PV contributed to data discussion, GR and AF performed experiments and contributed to data discussion, NF generated the TG mice and contributed to data discussion, GG contributed to data discussion, AG generated the TG mice and reviewed and discussed data and reviewed/edited the manuscript, MG reviewed and discussed data and reviewed/edited the manuscript, RB designed the study, reviewed data and wrote the manuscript, and acts as guarantor for the article. All authors gave final approval to the submitted manuscript.

Acknowledgements

This work was funded by the European Society for Clinical Nutrition and Metabolism (ESPEN) through a fellowship to GGC. The authors wish to thank Marco Stebel, M.Sc. and Davide Barbetta, DVM (Trieste University Animal Facility, Trieste, Italy) as well as Margherita De Nardo, MD and Lorenza Mamolo, MD (Dept. of Medical, Surgical and Health Sciences, University of Trieste, Italy) for excellent assistance in in vivo procedures. Manuela Boschelle, M.Sc. and Chiara Matilde Boccato, M.Sc. (Dept. of Medical, Surgical and Health Sciences, University of Trieste, Italy) are acknowledged for skilful technical assistance in ex vivo and in vitro experiments.

References

1. Bonnard C, Durand A, Peyrol S, Chanseaume E, Chauvin MA, Morio B, Vidal H, Rieusset J: Mitochondrial dysfunction results from oxidative stress in the skeletal muscle of diet-induced insulin-resistant mice. J Clin Invest 2008;118:789-800
2. Morino K, Petersen KF, Shulman GI: Molecular mechanisms of insulin resistance in humans and their potential links with mitochondrial dysfunction. Diabetes 2006;55 Suppl 2:S9-S15
3. Schenk S, Saberi M, Olefsky JM: Insulin sensitivity: modulation by nutrients and inflammation. J Clin Invest 2008;118:2992-3002
4. Victor VM, Espulgues JV, Hernandez-Mijares A, Rocha M: Oxidative stress and mitochondrial dysfunction in sepsis: a potential therapy with mitochondria-targeted antioxidants. Infect Disord Drug Targets 2009;9:376-389
5. Wei Y, Sowers JR, Clark SE, Li W, Ferrario CM, Stump CS: Angiotensin II-induced skeletal muscle insulin resistance mediated by NF-kappaB activation via NADPH oxidase. Am J Physiol Endocrinol Metab 2008;294:E345-351
6. Nakazato M, Murakami N, Date Y, Kojima M, Matsuo H, Kangawa K, Matsukura S: A role for ghrelin in the central regulation of feeding. Nature 2001;409:194-198
7. Chen CY, Asakawa A, Fujimiya M, Lee SD, Inui A: Ghrelin gene products and the regulation of food intake and gut motility. Pharmacol Rev 2009;61:430-481
8. Barazzoni R, Bosutti A, Stebel M, Cattin MR, Roder E, Visintin L, Cattin L, Biolo G, Zanetti M, Guarnieri G: Ghrelin regulates mitochondrial-lipid metabolism gene expression and tissue fat distribution in liver and skeletal muscle. Am J Physiol Endocrinol Metab 2005;288:E228-235
9. Barazzoni R, Zhu X, Deboer M, Datta R, Culler MD, Zanetti M, Guarnieri G, Marks DL: Combined effects of ghrelin and higher food intake enhance skeletal muscle mitochondrial oxidative capacity and AKT phosphorylation in rats with chronic kidney disease. Kidney Int 2010;77:23-28
10. Delhanty PJ, Neggers SJ, van der Lely AJ: Mechanisms in endocrinology: Ghrelin: the differences between acyl- and des-acyl ghrelin. Eur J Endocrinol 2012;167:601-608
11. Tschop M, Smiley DL, Heiman ML: Ghrelin induces adiposity in rodents. Nature 2000;407:908-913
12. Barazzoni R, Zanetti M, Ferreira C, Vinci P, Pirulli A, Mucci M, Dore F, Fonda M, Ciocchi B, Cattin L, Guarnieri G: Relationships between desacylated and acylated ghrelin and insulin sensitivity in the metabolic syndrome. J Clin Endocrinol Metab 2007;92:3935-3940
13. Barazzoni R, Gortan Cappellari G, Semolic A, Ius M, Mamolo L, Dore F, Giacca M, Zanetti M, Vinci P, Guarnieri G: Plasma total and unacylated ghrelin predict 5-year changes in insulin resistance. Clin Nutr. 2015;S0261-5614(15)00256-3
14. Dieci E, Casati L, Pagani F, Celotti F, Sibilia V: Acylated and unacylated ghrelin protect MC3T3-E1 cells against tert-butyl hydroperoxide-induced oxidative injury: pharmacological characterization of ghrelin receptor and possible epigenetic involvement. Amino Acids 2014;46:1715-1725
15. Togliatto G, Trombetta A, Dentelli P, Cotogni P, Rosso A, Tschop MH, Granata R, Ghigo E, Brizzi MF: Unacylated ghrelin promotes skeletal muscle regeneration following hindlimb ischemia via SOD-2-mediated miR-221/222 expression. J Am Heart Assoc 2013;2:e000376
16. Togliatto G, Trombetta A, Dentelli P, Gallo S, Rosso A, Cotogni P, Granata R, Falcioni R, Delale T, Ghigo E, Brizzi MF. Unacylated ghrelin induces oxidative stress resistance in a

glucose intolerance and peripheral artery disease mouse model by restoring endothelial cell miR-126 expression. Diabetes. 2015 Apr;64(4):1370-82.
17. Zhang Q, Huang WD, Lv XY, Yang YM: Ghrelin protects H9c2 cells from hydrogen peroxide-induced apoptosis through NF-kappaB and mitochondria-mediated signaling. Eur J Pharmacol 2011;654:142-149
18. Ryter SW, Koo JK, Choi AM: Molecular regulation of autophagy and its implications for metabolic diseases. Curr Opin Clin Nutr Metab Care 2014;17:329-337
19. Porporato PE, Filigheddu N, Reano S, Ferrara M, Angelino E, Gnocchi VF, Prodam F, Ronchi G, Fagoonee S, Fornaro M, Chianale F, Baldanzi G, Surico N, Sinigaglia F, Perroteau I, Smith RG, Sun Y, Geuna S, Graziani A: Acylated and unacylated ghrelin impair skeletal muscle atrophy in mice. J Clin Invest 2013;123:611-622
20. Lovric J, Mano M, Zentilin L, Eulalio A, Zacchigna S, Giacca M: Terminal differentiation of cardiac and skeletal myocytes induces permissivity to AAV transduction by relieving inhibition imposed by DNA damage response proteins. Mol Ther 2012;20:2087-2097
21. Gortan Cappellari G, Losurdo P, Mazzucco M, Panizon E, Jevnicar M, Macaluso L, Fabris B, Barazzoni R, Biolo G, Carretta R, Zanetti M: Treatment with n-3 polyunsaturated fatty acids reverses endothelial dysfunction and oxidative stress in experimental menopause. J Nutr Biochem 2013;24:371-379
22. Barazzoni R, Zanetti M, Gortan Cappellari G, Semolic A, Boschelle M, Codarin E, Pirulli A, Cattin L, Guarnieri G: Fatty acids acutely enhance insulin-induced oxidative stress and cause insulin resistance by increasing mitochondrial reactive oxygen species (ROS) generation and nuclear factor-kappaB inhibitor (IkappaB)-nuclear factor-kappaB (NFkappaB) activation in rat muscle, in the absence of mitochondrial dysfunction. Diabetologia 2012;55:773-782
23. Barazzoni R, Zanetti M, Bosutti A, Biolo G, Vitali-Serdoz L, Stebel M, Guarnieri G: Moderate caloric restriction, but not physiological hyperleptinemia per se, enhances mitochondrial oxidative capacity in rat liver and skeletal muscle--tissue-specific impact on tissue triglyceride content and AKT activation. Endocrinology 2005;146:2098-2106
24. Rahman I, Kode A, Biswas SK: Assay for quantitative determination of glutathione and glutathione disulfide levels using enzymatic recycling method. Nat Protoc 2006;1:3159-3165
25. Zanetti M, Gortan Cappellari G, Burekovic I, Barazzoni R, Stebel M, Guarnieri G: Caloric restriction improves endothelial dysfunction during vascular aging: Effects on nitric oxide synthase isoforms and oxidative stress in rat aorta. Exp Gerontol 2010;45:848-855
26. Yamamoto N, Kawasaki K, Kawabata K, Ashida H: An enzymatic fluorimetric assay to quantitate 2-deoxyglucose and 2-deoxyglucose-6-phosphate for in vitro and in vivo use. Anal Biochem 2010;404:238-240
27. Clerk LH, Rattigan S, Clark MG: Lipid infusion impairs physiologic insulin-mediated capillary recruitment and muscle glucose uptake in vivo. Diabetes 2002;51:1138-1145
28. Bonen A, Tan MH, Watson-Wright WM: Insulin binding and glucose uptake differences in rodent skeletal muscles. Diabetes 1981;30:702-704
29. Lanza IR, Nair KS: Functional Assessment of Isolated Mitochondria In Vitro. Methods Enzymol. 2009;457:349-372
30. Cao S, Zhang X, Edwards JP, Mosser DM: NF-kappaB1 (p50) homodimers differentially regulate pro- and anti-inflammatory cytokines in macrophages. J Biol Chem 2006;281:26041-50
31. Hancer NJ, Qiu W, Cherella C, Li Y, Copps KD, White MF: Insulin and metabolic stress stimulate multisite serine/threonine phosphorylation of insulin receptor substrate 1 and inhibit tyrosine phosphorylation. J Biol Chem 2014;289:12467-12484

32. Barazzoni R, Zanetti M, Cattin MR, Visintin L, Vinci P, Cattin L, Stebel M, Guarnieri G: Ghrelin enhances in vivo skeletal muscle but not liver AKT signaling in rats. Obesity (Silver Spring) 2007;15:2614-2623
33. Gortan Cappellari G, Zanetti M, Semolic A, Vinci P, Ruozi G, De Nardo M, Filigheddu N, Guarnieri G, Giacca M, Graziani A, Barazzoni R: Unacylated ghrelin does not alter mitochondrial function, redox state and triglyceride content in rat liver in vivo. Clin Nutr Exp 2015;4:1-7
34. Filigheddu N, Gnocchi VF, Coscia M, Cappelli M, Porporato PE, Taulli R, Traini S, Baldanzi G, Chianale F, Cutrupi S, Arnoletti E, Ghe C, Fubini A, Surico N, Sinigaglia F, Ponzetto C, Muccioli G, Crepaldi T, Graziani A: Ghrelin and des-acyl ghrelin promote differentiation and fusion of C2C12 skeletal muscle cells. Mol Biol Cell 2007;18:986-994
35. Ruozi G, Bortolotti F, Falcione A, Dal Ferro M, Ukovich L, Macedo A, Zentilin L, Filigheddu N, Gortan Cappellari G, Baldini G, Zweyer M, Barazzoni R, Graziani A, Zacchigna S, Giacca M. AAV-mediated in vivo functional selection of tissue-protective factors against ischaemia. Nat Commun. 2015 Jun 11;6:7388
36. Barbieri E, Sestili P: Reactive oxygen species in skeletal muscle signaling. J Signal Transduct 2012;2012:982794
37. Soraru G, Vergani L, Fedrizzi L, D'Ascenzo C, Polo A, Bernazzi B, Angelini C: Activities of mitochondrial complexes correlate with nNOS amount in muscle from ALS patients. Neuropathol Appl Neurobiol 2007;33:204-211
38. Brookes PS, Levonen AL, Shiva S, Sarti P, Darley-Usmar VM: Mitochondria: regulators of signal transduction by reactive oxygen and nitrogen species. Free Radic Biol Med 2002;33:755-764
39. Granata R, Settanni F, Biancone L, Trovato L, Nano R, Bertuzzi F, Destefanis S, Annunziata M, Martinetti M, Catapano F, Ghe C, Isgaard J, Papotti M, Ghigo E, Muccioli G: Acylated and unacylated ghrelin promote proliferation and inhibit apoptosis of pancreatic beta-cells and human islets: involvement of 3',5'-cyclic adenosine monophosphate/protein kinase A, extracellular signal-regulated kinase 1/2, and phosphatidyl inositol 3-Kinase/Akt signaling. Endocrinology 2007;148:512-529
40. Liu Y, Palanivel R, Rai E, Park M, Gabor TV, Scheid MP, Xu A, Sweeney G: Adiponectin stimulates autophagy and reduces oxidative stress to enhance insulin sensitivity during high-fat diet feeding in mice. Diabetes 2015;64:36-48
41. Holloszy JO: "Deficiency" of mitochondria in muscle does not cause insulin resistance. Diabetes 2013;62:1036-1040
42. Fisher-Wellman KH, Weber TM, Cathey BL, Brophy PM, Gilliam LA, Kane CL, Maples JM, Gavin TP, Houmard JA, Neufer PD: Mitochondrial respiratory capacity and content are normal in young insulin-resistant obese humans. Diabetes 2014;63:132-141
43. Nair KS, Bigelow ML, Asmann YW, Chow LS, Coenen-Schimke JM, Klaus KA, Guo ZK, Sreekumar R, Irving BA: Asian Indians have enhanced skeletal muscle mitochondrial capacity to produce ATP in association with severe insulin resistance. Diabetes 2008;57:1166-1175
44. Sreekumar R, Unnikrishnan J, Fu A, Nygren J, Short KR, Schimke J, Barazzoni R, Nair KS. Impact of high-fat diet and antioxidant supplement on mitochondrial functions and gene transcripts in rat muscle. Am J Physiol Endocrinol Metab. 2002 May;282(5):E1055-61
45. Barazzoni R. Skeletal muscle mitochondrial protein metabolism and function in ageing and type 2 diabetes. Curr Opin Clin Nutr Metab Care 2004 Jan;7(1):97-102

46. Fink BD, O'Malley Y, Dake BL, Ross NC, Prisinzano TE, Sivitz WI: Mitochondrial targeted coenzyme Q, superoxide, and fuel selectivity in endothelial cells. PLoS One 2009;4:e4250
47. Anderson EJ, Yamazaki H, Neufer PD: Induction of endogenous uncoupling protein 3 suppresses mitochondrial oxidant emission during fatty acid-supported respiration. J Biol Chem 2007;282:31257-31266
48. St-Pierre J, Buckingham JA, Roebuck SJ, Brand MD: Topology of superoxide production from different sites in the mitochondrial electron transport chain. J Biol Chem 2002;277:44784-44790

Figure Legends

Figure 1. **UnAG and skeletal muscle redox state.** Effects of unacylated ghrelin (UnAG, 200µg subcutaneous injection twice per day) vs. saline (Ct) sustained 4-day treatment on overall (A) and specific superoxide production from mitochondrial sources in whole tissue homogenate (B), on intact isolated mitochondrial H_2O_2 synthesis rate with different respiratory substrates (C, GMS: Glutamate+Succinate+Malate; S: Succinate; GM: Glutamate+Malate; PCM: Palmitoyl-L-Carnintine+Malate) and on superoxide generation from nitric oxide synthase (D), NADPH oxidase (E) and xanthine oxidase (F) in skeletal muscle. Effects of UnAG treatment on total (G) and oxidized (GSSG) over total (H, GSH: reduced) tissue glutathione, effects of UnAG on protein expression of Cu/ZnSOD (I) and MnSOD (J) with representative blots, and on enzyme activities of catalase (K) and glutathione peroxidase (GPx; L). U CS: units of citrate synthase; a.u.: arbitrary units. *$p<0.05$ vs. Ct; mean±SEM, n=8-10/group.

Figure 2. **UnAG and skeletal muscle inflammation.** Effects of unacylated ghrelin (UnAG, 200µg subcutaneous injection twice per day) vs. saline (Ct) sustained 4-day treatment on the expression of IκB (A), on NF-κB binding activity (B) with representative blots, and on tissue expression of IL-1α (C), IL-1β (D), TNFα (E), IL-6 (F) and IL-10 (G) measured by xMAP technology in gastrocnemious muscle. a.u.: arbitrary units, Ab: antibody. *$p<0.05$ vs. Ct; mean±SEM; n=8-10/group.

Figure 3. **UnAG and skeletal muscle insulin action.** Effects of unacylated ghrelin (UnAG, 200µg subcutaneous injection twice per day) vs. saline (Ct) sustained 4-day treatment on the phosphorylation measured by xMAP technology of insulin receptor ($IR^{Y1162/Y1163}$, A), IRS-1^{S312} (B), AKT^{S473} (C), GSK-$3\beta^{S9}$ (D), $PRAS40^{T246}$ (E), $P70S6K^{T421/S424}$ (F) and on tissue glucose uptake (G)

in gastrocnemious muscle. *p<0.05 vs. Ct; †p<0.05 vs. same treatment Insulin-; ‡p<0.05 vs. other treatment Insulin-; mean±SEM, n=8-10/group.

Figure 4. **Impact of systemic overexpression of UnAG on skeletal muscle redox state, inflammation, insulin signaling and action in lean and obese mice.** Effects of UnAG overexpression in transgenic Myh6/Ghrl (Tg) vs. wild type (Wt) mice fed 16 wks with Control- (CD) or High Fat- Diet (HFD) on total (A) and oxidized (GSSG) over total (B, GSH: reduced) glutathione, on tissue expression of IL-1α (C), IL-1β (D), TNFα (E), IL-6 (F) and IL-10 (G) measured by xMAP technology in gastrocnemius muscle. Effects of UnAG overexpression on the phosphorylation of insulin receptor ($IR^{Y1162/Y1163}$, H), IRS-1^{S312} (I), AKT^{S473} (J), GSK-$3\beta^{S9}$ (K), $PRAS40^{T246}$ (L), $P70S6K^{T421/S424}$ (M) measured by xMAP technology in gastrocnemius muscle. Absolute (N), corresponding Area Under the Curve (AUC; O), and relative (P) blood glucose values in Insulin Tolerance Test (ITT) experiments. *p<0.05 vs. Ct; †p<0.05 vs. same genotype-CD; ‡p<0.05 vs. other genotype-CD; mean±SEM, n=7/group.

Figure 5. **In vitro impact of UnAG on cultured myotubes.** Effects of 48 h incubation with increasing concentrations of acylated (AG) or unacylated ghrelin (UnAG) vs. control (Ct) on isolated mitochondria H_2O_2 synthesis rate with different respiratory substrates (A, GMS: Glutamate+Succinate+Malate; S: Succinate; GM: Glutamate+Malate; PCM: Palmitoyl-L-Carnintine+Malate) and effects of the above treatments on the phosphorylation of insulin receptor $(IR)^{Y1162/Y1163}$ (B), IRS-1^{S312} (C), AKT^{S473} (D), GSK-$3\beta^{S9}$ (E), $PRAS40^{T246}$ (F), $P70S6K^{T421/S424}$ (G) measured by xMAP technology in C2C12 myotubes. U CS: units of citrate synthase. *p<0.05 vs. Ct; †p<0.05 vs. same hormone 0.1μM; ‡p<0.05 vs. same hormone 0.5μM; § p<0.05 vs. AG, same concentration; $p<0.05 vs. other hormone 0.5μM; ¶p<0.05 vs. other hormone 0.1μM; #p<0.05 vs. all other groups; mean±SEM, n=3/group.

Figure 6. **Impact of UnAG on mitochondrial ATP synthesis.** Effects on muscle ATP synthesis rate with different respiratory substrates (A, PPKM: Pyruvate+Palmitoyl-L-Carnintine+α-Ketoglutarate+Malate; PCM: Palmitoyl-L-Carnintine+Malate; GM: Glutamate+Malate; SR: Succinate+Rotenone) in isolated mitochondria from rat gastrocnemious muscle after unacylated ghrelin (UnAG, 200µg subcutaneous injection twice per day) vs. saline (Ct) sustained 4-day (A, n=8-10/group) treatment, in isolated mitochondria from gastrocnemious muscle of mice with UnAG up-regulation (Tg Myh6/Ghrl) vs. wild type (wt) fed 16 wks with Control- (CD) or High Fat- Diet (HFD) (B, n=7/group) and in C2C12 myotubes after 48 h incubation with increasing concentrations of acylated (AG) or unacylated ghrelin (UnAG) vs. control (Ct) in (C, n=3/treatment). Complex I over complex II related ATP synthesis rate ratio in rat gastrocnemius muscle after sustained treatment (D) and in cultured myotubes (E). *$p<0.05$ vs. Ct or Wt; †$p<0.05$ vs. same genotype-CD; ‡$p<0.05$ vs. other genotype-CD; § $p<0.05$ vs. AG, same concentration; #$p<0.05$ vs. all other groups; mean±SEM.

Figure 7. **Role of autophagy in UnAG effects on mitochondrial ROS generation and insulin signalling.** Effects of autophagy mediator ATG5 genomic silencing vs. non targeting NT4 siRNA transfection on C2C12 myotubes after 48 h incubation with increasing concentrations of acylated (AG) or unacylated ghrelin (UnAG) vs. control (Ct) on isolated mitochondria H_2O_2 synthesis rate with different respiratory substrates (A, GMS: Glutamate+Succinate+Malate; S: Succinate; GM: Glutamate+Malate; PCM: Palmitoyl-L-Carnintine+Malate) and cell protein expression of ATG5 after transfection with the two siRNA (B). Effects of the above treatments on the phosphorylation of insulin receptor $(IR)^{Y1162/Y1163}$ (C), $IRS\text{-}1^{S312}$ (D), AKT^{S473} (E), $GSK\text{-}3\beta^{S9}$ (F), $PRAS40^{T246}$ (G), $P70S6K^{T421/S424}$ (H) measured by xMAP technology. Autophagy activation marker LC3II/LC3I as measured by western blot in the gastrocnemious muscle of mice with UnAG up-regulation (Tg

Myh6/Ghrl) vs. wild type (wt) fed 16 wks with Control- (CD) or High Fat- Diet (HFD) (I, n=7/group) with representative blot. U CS: units of citrate synthase. *p<0.05 vs. NT4, same UnAG concentration; †p<0.05 vs. same siRNA, no UnAG; ‡p<0.05 vs. other siRNA, no UnAG; § p<0.05 vs. same siRNA, UnAG 0.1μM; § p<0.05 vs. other siRNA, UnAG 0.1μM; #p<0.05 vs. all other groups; mean±SEM; n=3/group.

Figure 8: Proposed interactions between UnAG and clustered obesity-associated metabolic alterations in skeletal muscle of high-fat diet-induced obese rodents: higher mitochondrial production of reactive oxygen species (ROS), higher inflammation and lower insulin signalling activation are normalized by chronic UnAG over-exposure. Our findings further demonstrate a direct effect of UnAG to lower mitochondrial ROS production through stimulated autophagy, which may directly lead to lower inflammation and enhanced insulin signalling. Potential parallel UnAG activities to directly lower inflammation and enhance insulin signalling should be further investigated.

Supplementary Figure Legends

Supplementary Figure 1. **UnAG and IRS-1^{Y612} phosphorylation in skeletal muscle.** Effects of unacylated ghrelin (UnAG, 200µg subcutaneous injection twice per day) vs. saline (Ct) sustained 4-day treatment (A, n=8-10/group), or of UnAG up-regulation in transgenic Myh6/Ghrl (Tg) vs. wild type (Wt) mice fed 16 wks with Control- (CD) or High Fat- Diet (HFD) (B, n=7/group) on the phosphorylation of IRS-1^{Y612} in gastrocnemius muscle with representative blots. OD: optical density. Mean±SEM.

Supplementary Figure 2. **UnAG and liver redox state and inflammation.** Effects of unacylated ghrelin (UnAG, 200µg subcutaneous injection twice per day) vs. saline (Ct) sustained 4-day treatment on overall (A) and specific superoxide production from mitochondrial sources in whole tissue homogenate (B), on intact isolated mitochondria H_2O_2 synthesis rate with different respiratory substrates (C, GMS: Glutamate+Succinate+Malate; S: Succinate; GM: Glutamate+Malate; PCM: Palmitoyl-L-Carnintine+Malate) and on superoxide generation from nitric oxide synthase (D), NADPH oxidase (E) and xanthine oxidase (F) in rat liver. Effects of UG treatment on total (G) and oxidized (GSSG) over total (H, GSH: reduced) tissue glutathione, and on the binding activity of NF-κB (I), with representative blot, in rat liver. U CS: units of citrate synthase; a.u.: arbitrary units, Ab: antibody. Mean±SEM, n=8-10/group.

Supplementary Figure 3. **UnAG and liver insulin action and ATP synthesis.** Effects of unacylated ghrelin (UnAG, 200µg subcutaneous injection twice per day) vs. saline (Ct) sustained 4-day treatment on the phosphorylation of insulin receptor (IR)$^{Y1162/Y1163}$ (A), IRS-1^{S312} (B), AKT^{S473} (C), GSK-3β^{S9} (D), PRAS40^{T246} (E), P70S6K$^{T421/S424}$ (F) measured by xMAP technology, and on isolated mitochondrial ATP synthesis rate with different respiratory

substrates (E, PPKM: Pyruvate+Palmitoyl-L-Carnintine+α-Ketoglutarate+Malate; PCM: Palmitoyl-L-Carnintine+Malate; GM: Glutamate+Malate; SR: Succinate+Rotenone) in rat liver. Mean±SEM, n=8-10/group.

Figure 1

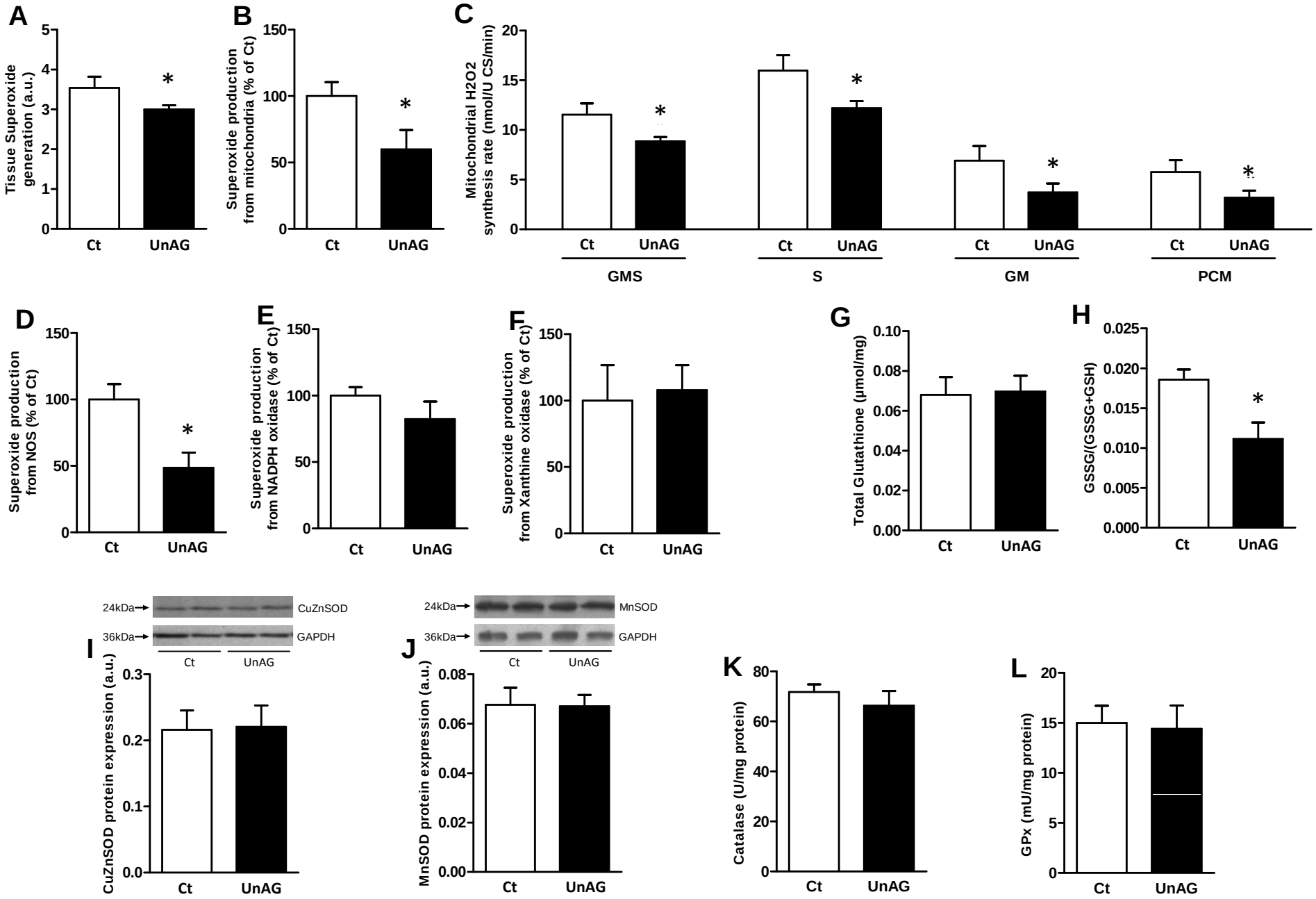
A
Tissue Superoxide generation (a.u.)
Ct
UnAG
B
Superoxide production from mitochondria (% of Ct)
C
Mitochondrial H2O2 synthesis rate (nmol/U CS/min)
GMS
S
GM
PCM
D
Superoxide production from NOS (% of Ct)
E
Superoxide production from NADPH oxidase (% of Ct)
F
Superoxide production from Xanthine oxidase (% of Ct)
G
Total Glutathione (µmol/mg)
H
GSSG/(GSSG+GSH)
24kDa
CuZnSOD
36kDa
GAPDH
I
CuZnSOD protein expression (a.u.)
MnSOD
J
MnSOD protein expression (a.u.)
K
Catalase (U/mg protein)
L
GPx (mU/mg protein)

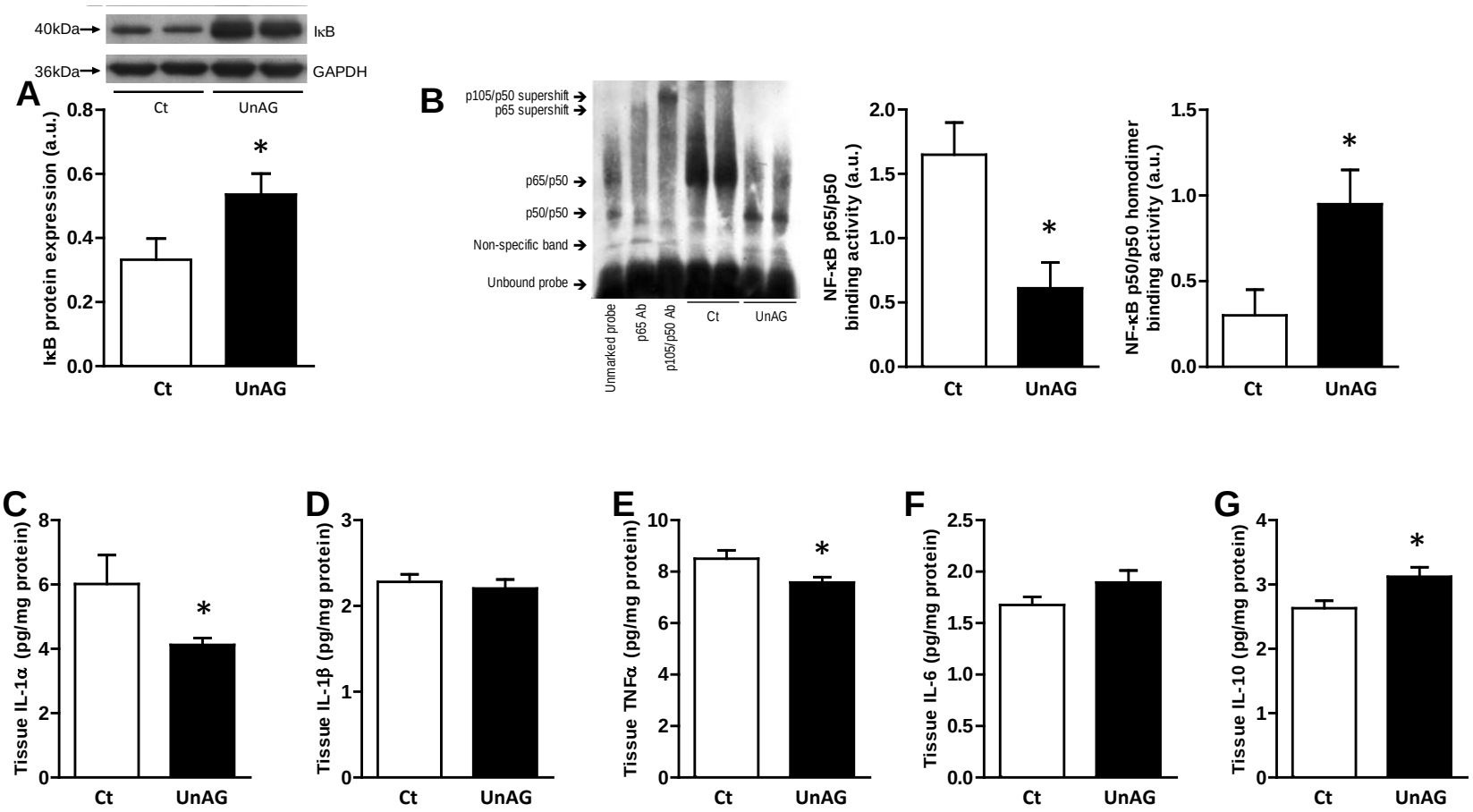
40kDa
IκB
36kDa
GAPDH
A
Ct
UnAG
IκB protein expression (a.u.)
0.8
0.6
0.4
0.2
0.0
*
Ct
UnAG
B
p105/p50 supershift
p65 supershift
p65/p50
p50/p50
Non-specific band
Unbound probe
Unmarked probe
p65 Ab
p105/p50 Ab
Ct
UnAG
NF-κB p65/p50 binding activity (a.u.)
2.0
1.5
1.0
0.5
0.0
*
Ct
UnAG
NF-κB p50/p50 homodimer binding activity (a.u.)
1.5
1.0
0.5
0.0
*
Ct
UnAG
C
Tissue IL-1α (pg/mg protein)
8
6
4
2
0
*
Ct
UnAG
D
Tissue IL-1β (pg/mg protein)
3
2
1
0
Ct
UnAG
E
Tissue TNFα (pg/mg protein)
10
8
6
4
2
0
*
Ct
UnAG
F
Tissue IL-6 (pg/mg protein)
2.5
2.0
1.5
1.0
0.5
0.0
Ct
UnAG
G
Tissue IL-10 (pg/mg protein)
4
3
2
1
0
*
Ct
UnAG

Figure 3

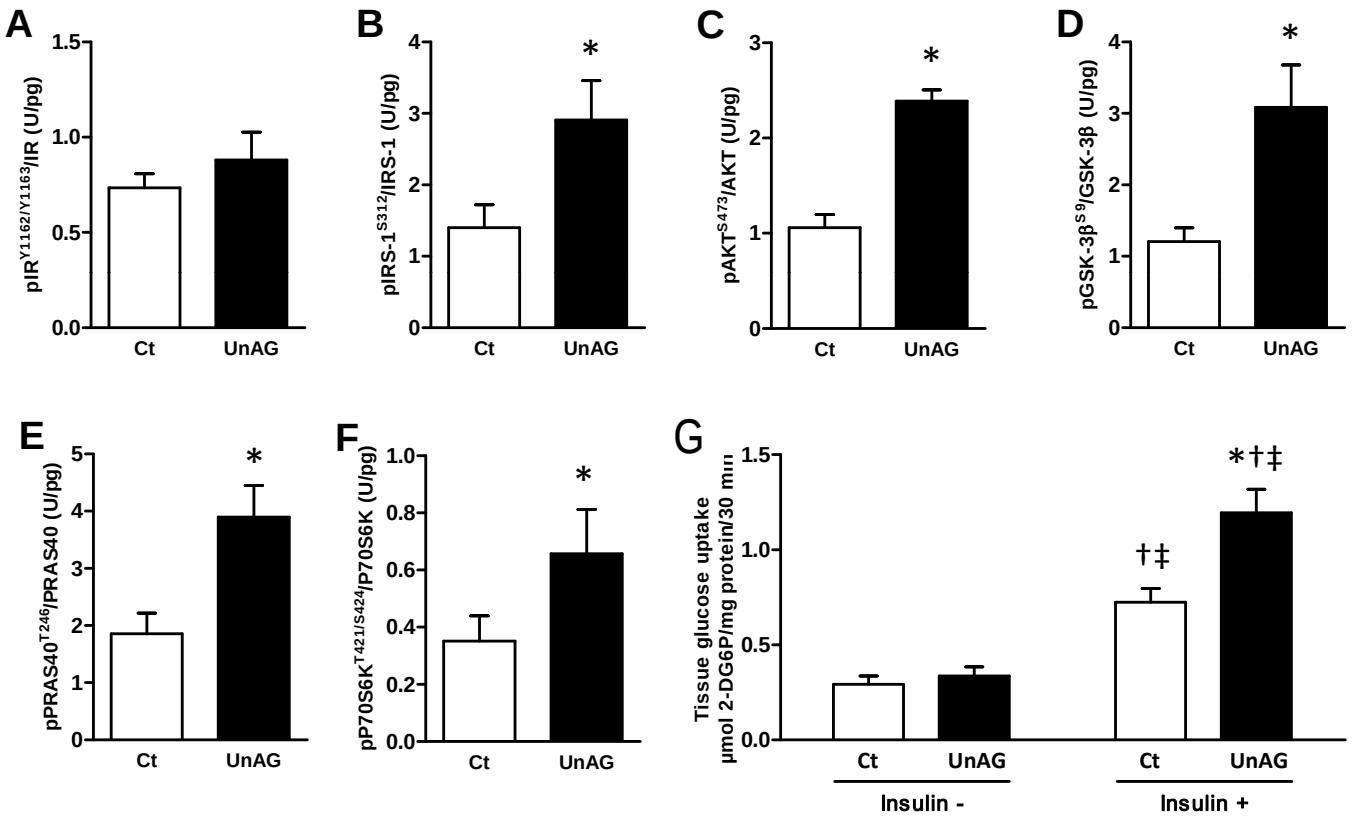
A
pIR$^{Y1162/Y1163}$/IR (U/pg)
1.5
1.0
0.5
0.0
Ct
UnAG
B
pIRS-1^{S312}/IRS-1 (U/pg)
4
3
2
1
0
*
Ct
UnAG
C
pAKT^{S473}/AKT (U/pg)
3
2
1
0
*
Ct
UnAG
D
pGSK-3β^{S9}/GSK-3β (U/pg)
4
3
2
1
0
*
Ct
UnAG
E
pPRAS40^{T246}/PRAS40 (U/pg)
5
4
3
2
1
0
*
Ct
UnAG
F
pP70S6K$^{T421/S424}$/P70S6K (U/pg)
1.0
0.8
0.6
0.4
0.2
0.0
*
Ct
UnAG
G
Tissue glucose uptake
µmol 2-DG6P/mg protein/30 min
1.5
1.0
0.5
0.0
†‡
*†‡
Ct
UnAG
Ct
UnAG
Insulin -
Insulin +

Figure 4

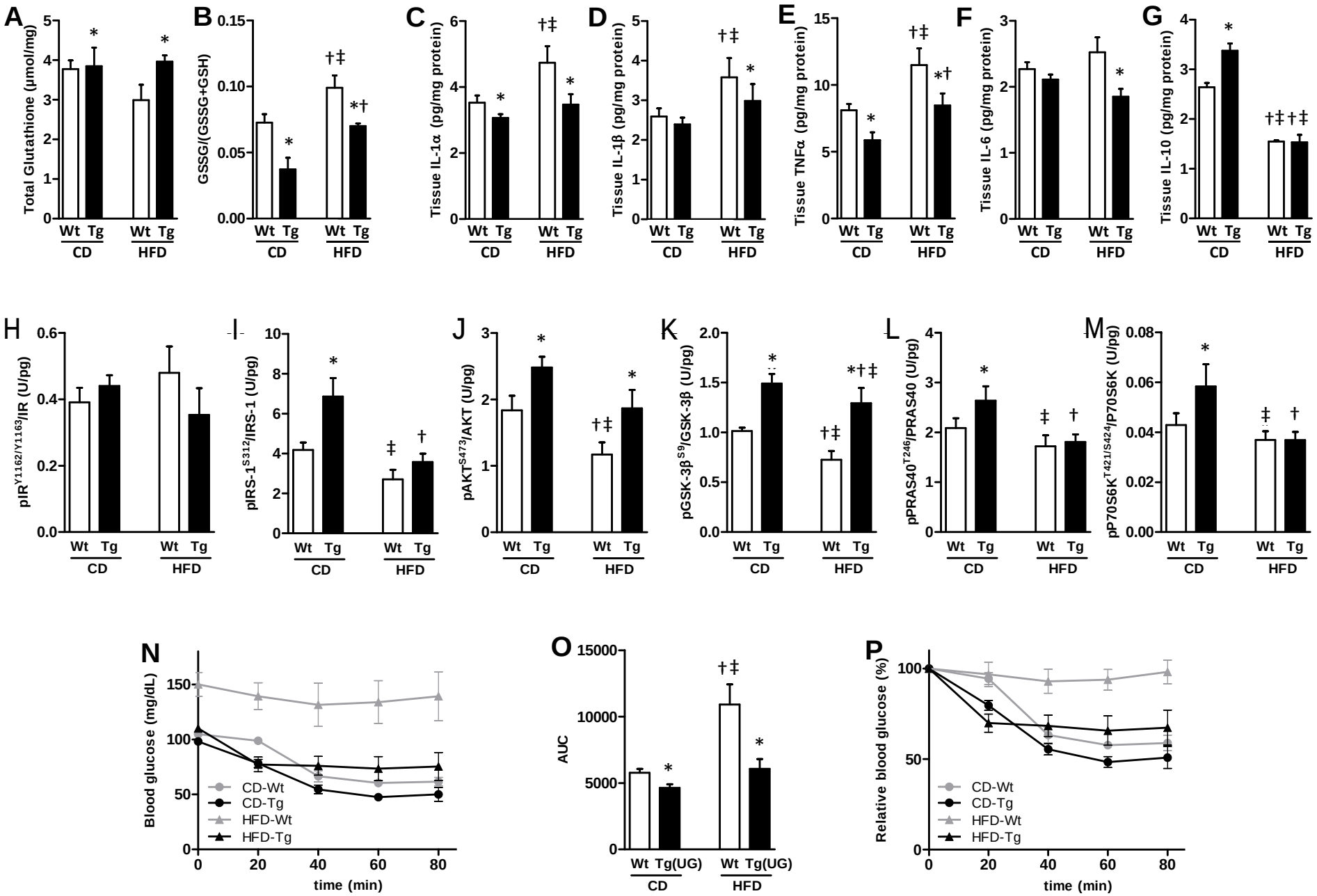
A
Total Glutathione (µmol/mg)
B
GSSG/(GSSG+GSH)
C
Tissue IL-1α (pg/mg protein)
D
Tissue IL-1β (pg/mg protein)
E
Tissue TNFα (pg/mg protein)
F
Tissue IL-6 (pg/mg protein)
G
Tissue IL-10 (pg/mg protein)
H
pIR$^{Y1162/Y1163}$/IR (U/pg)
I
pIRS-1^{S312}/IRS-1 (U/pg)
J
pAKT^{S473}/AKT (U/pg)
K
pGSK-3β^{S9}/GSK-3β (U/pg)
L
pPRAS40^{T246}/PRAS40 (U/pg)
M
pP70S6K$^{T421/S424}$/P70S6K (U/pg)
Wt Tg
CD
HFD
N
Blood glucose (mg/dL)
time (min)
CD-Wt
CD-Tg
HFD-Wt
HFD-Tg
O
AUC
Wt Tg(UG)
P
Relative blood glucose (%)

Figure 5

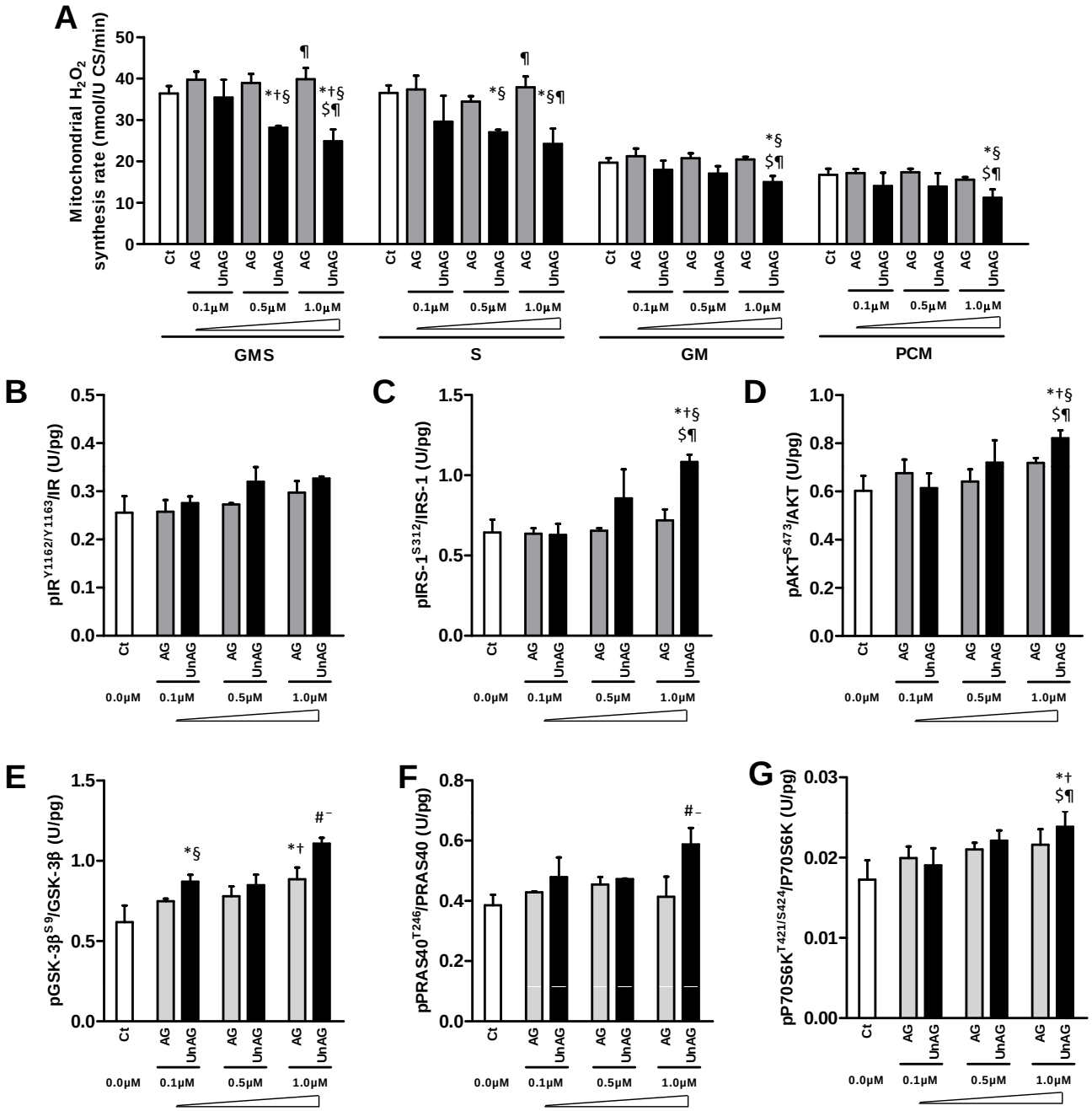
A
Mitochondrial H_2O_2 synthesis rate (nmol/U CS/min)
Ct
AG
UnAG
0.1μM
0.5μM
1.0μM
GMS
S
GM
PCM
B
$pIR^{Y1162/Y1163}/IR$ (U/pg)
C
$pIRS\text{-}1^{S312}/IRS\text{-}1$ (U/pg)
D
$pAKT^{S473}/AKT$ (U/pg)
0.0μM
E
$pGSK\text{-}3\beta^{S9}/GSK\text{-}3\beta$ (U/pg)
F
$pPRAS40^{T246}/PRAS40$ (U/pg)
G
$pP70S6K^{T421/S424}/P70S6K$ (U/pg)

Figure 6

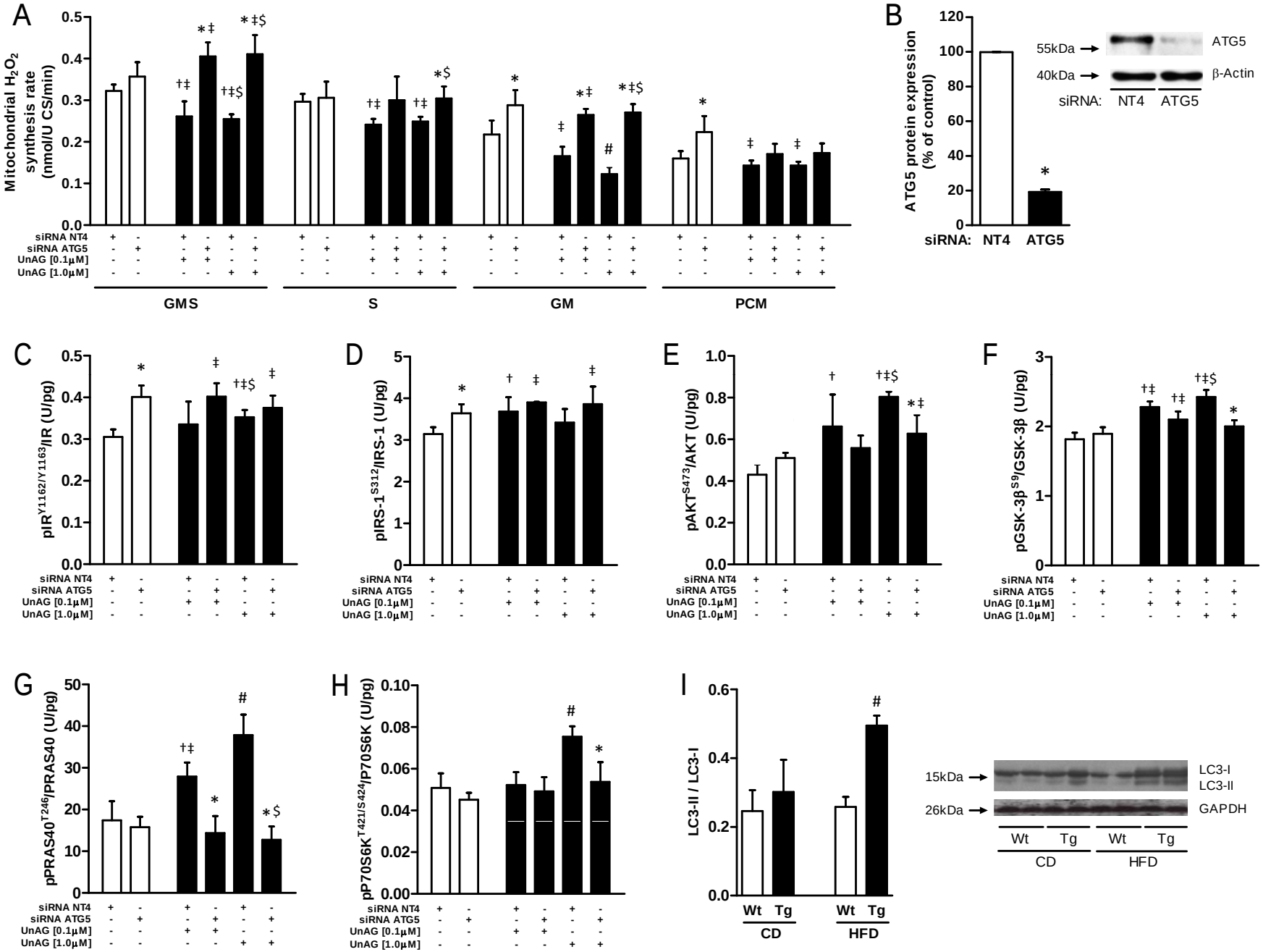
A
Mitochondrial H2O2 synthesis rate (nmol/U CS/min)
siRNA NT4
siRNA ATG5
UnAG [0.1μM]
UnAG [1.0μM]
GMS
S
GM
PCM
B
ATG5 protein expression (% of control)
siRNA: NT4 ATG5
55kDa
40kDa
ATG5
β-Actin
siRNA: NT4 ATG5
C
pIRY1162/Y1163/IR (U/pg)
D
pIRS-1S312/IRS-1 (U/pg)
E
pAKTS473/AKT (U/pg)
F
pGSK-3βS9/GSK-3β (U/pg)
G
pPRAS40T246/PRAS40 (U/pg)
H
pP70S6KT421/S424/P70S6K (U/pg)
I
LC3-II / LC3-I
Wt Tg Wt Tg
CD HFD
15kDa
26kDa
LC3-I
LC3-II
GAPDH
Wt Tg Wt Tg
CD HFD

Figure 7

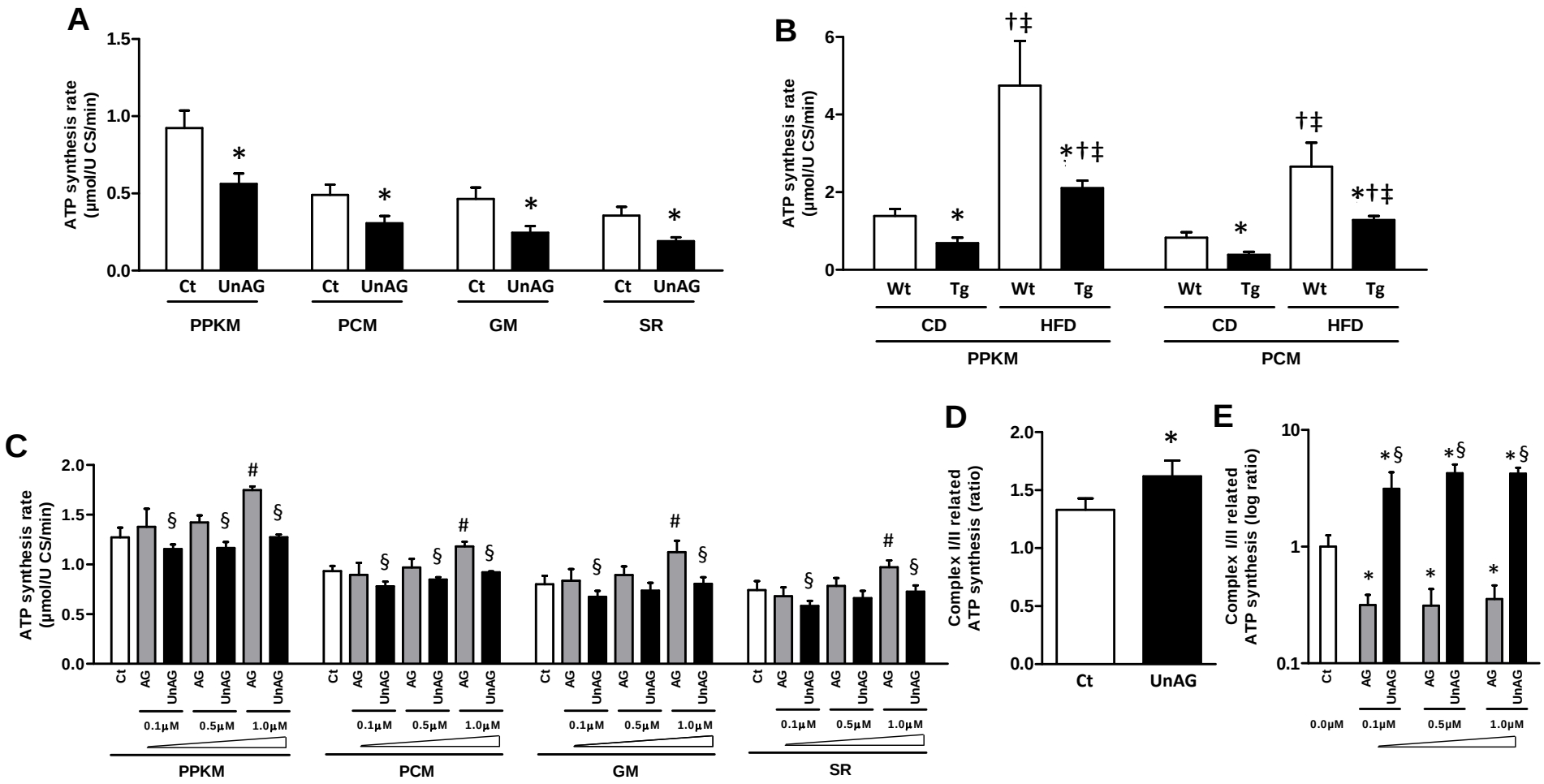
A
ATP synthesis rate (µmol/U CS/min)
1.5
1.0
0.5
0.0
Ct
UnAG
PPKM
PCM
GM
SR
B
ATP synthesis rate (µmol/U CS/min)
6
4
2
0
Wt
Tg
CD
HFD
PPKM
PCM
C
ATP synthesis rate (µmol/U CS/min)
2.0
1.5
1.0
0.5
0.0
Ct
AG
UnAG
0.1µM
0.5µM
1.0µM
PPKM
PCM
GM
SR
D
Complex I/II related ATP synthesis (ratio)
2.0
1.5
1.0
0.5
0.0
Ct
UnAG
E
Complex I/II related ATP synthesis (log ratio)
10
1
0.1
Ct
AG
UnAG
0.0µM
0.1µM
0.5µM
1.0µM

Figure 8

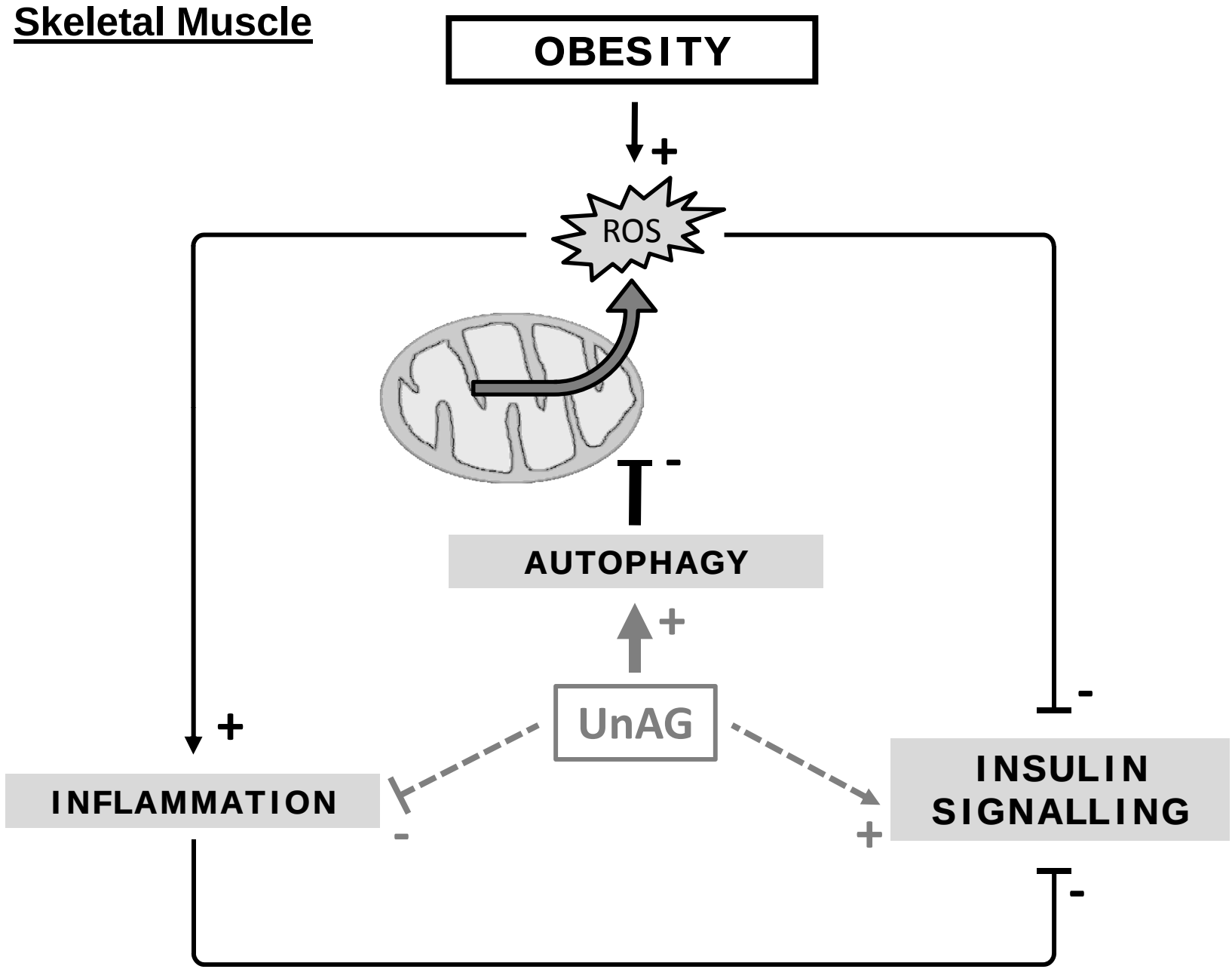
Skeletal Muscle
OBESITY
+
ROS
-
AUTOPHAGY
+
UnAG
+
INFLAMMATION
-
-
INSULIN SIGNALLING
+
-

Supplementary figure 1

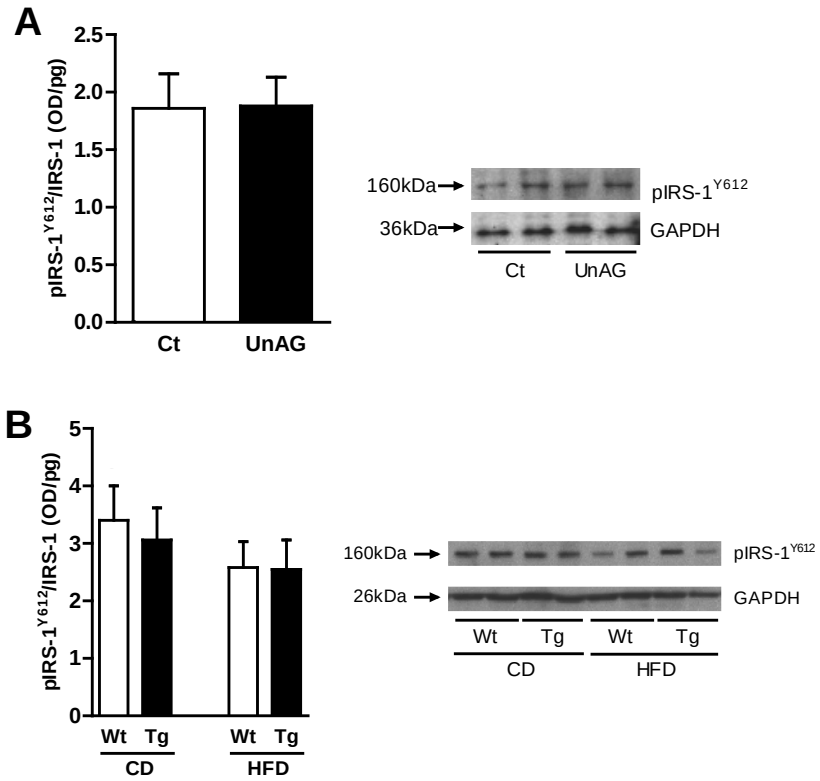

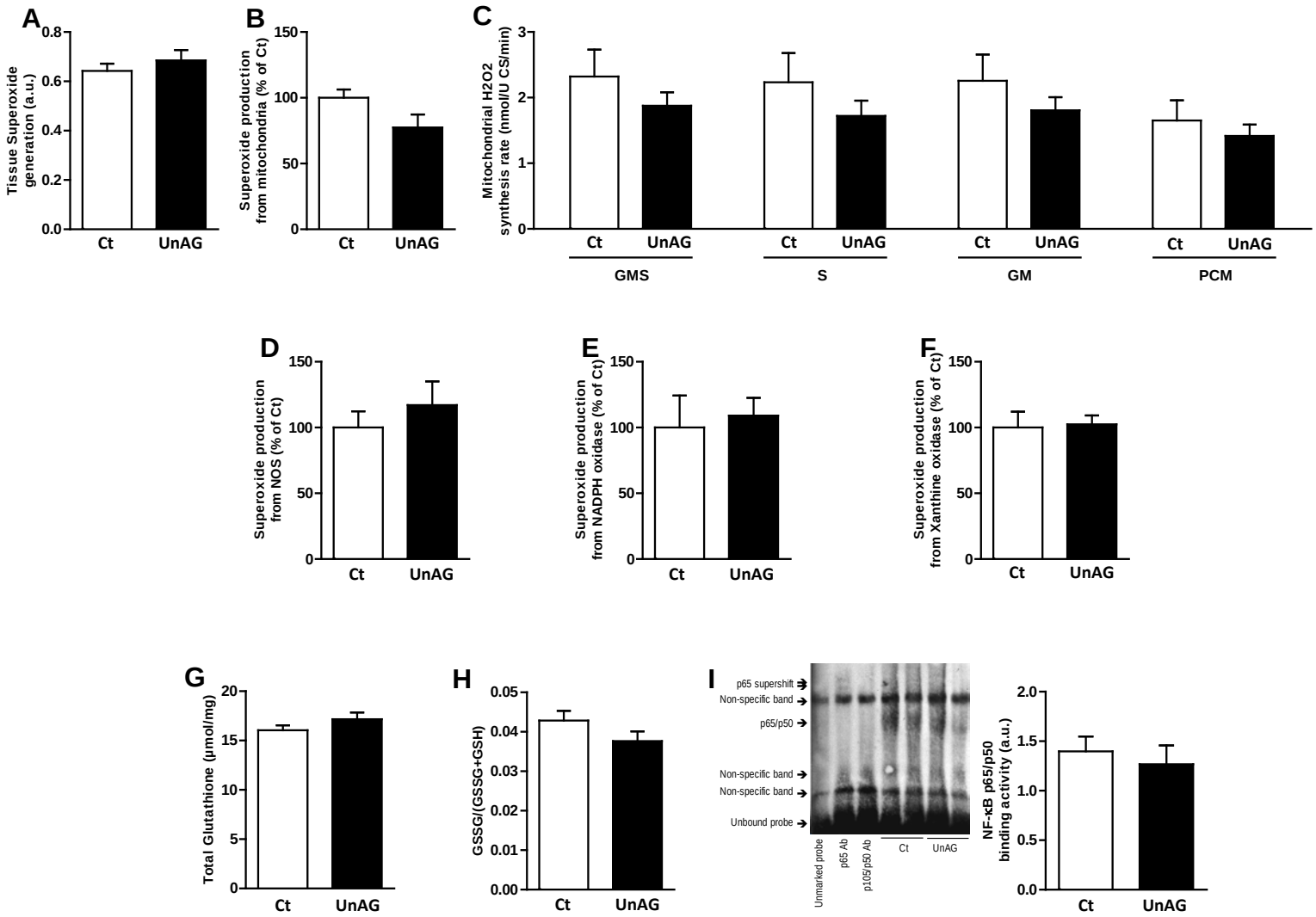
A
Tissue Superoxide generation (a.u.)
0.0
0.2
0.4
0.6
0.8
Ct
UnAG
B
Superoxide production from mitochondria (% of Ct)
0
50
100
150
Ct
UnAG
C
Mitochondrial H2O2 synthesis rate (nmol/U CS/min)
0
1
2
3
Ct
UnAG
GMS
S
GM
PCM
D
Superoxide production from NOS (% of Ct)
0
50
100
150
Ct
UnAG
E
Superoxide production from NADPH oxidase (% of Ct)
0
50
100
150
Ct
UnAG
F
Superoxide production from Xanthine oxidase (% of Ct)
0
50
100
150
Ct
UnAG
G
Total Glutathione (µmol/mg)
0
5
10
15
20
Ct
UnAG
H
GSSG/(GSSG+GSH)
0.00
0.01
0.02
0.03
0.04
0.05
Ct
UnAG
I
p65 supershift
Non-specific band
p65/p50
Non-specific band
Non-specific band
Unbound probe
Unmarked probe
p65 Ab
p105/p50 Ab
Ct
UnAG
NF-κB p65/p50 binding activity (a.u.)
0.0
0.5
1.0
1.5
2.0
Ct
UnAG

Supplementary figure 3